Enhancing subbasalt reflections using parabolic τ-p transformation

ROMAN SPITZER and ROBERT S. WHITE, University of Cambridge, U.K.
PHILIP A. F. CHRISTIE, Schlumberger Cambridge Research, U.K.

Potential hydrocarbon-bearing sediment structures in the Faroe-Shetland Basin are often overlain by basaltic sequences of stacked flows up to several kilometers thick. With conventional seismic acquisition and processing methods, it is difficult to image the internal (intrabasalt) and underlying (subbasalt) structures. Scattering from the highly reflective top of the basalt and short-period multiples from intrabasalt boundaries may completely mask reflections from the base of the basalt and below. High attenuation of seismic energy in the basaltic sequence due to its complex internal structure generally causes a weak subbasalt signal. Long-period multiples, such as those generated between the sea bottom and the top-basalt boundary, may obscure subbasalt reflections and energy reflected from the basement.

Recent investigations have shown that integrated near-offset and wide-angle acquisition (e.g., Fruehn et al., 2001) combined with a broadband, low-frequency source (Ziolkowski et al., 2003) have the potential to overcome some of the aforementioned difficulties. Application of model-based processing (e.g., Hanssen et al., 2003) and inversion techniques (Fruehn et al., 1998) are useful for identifying weak subbasalt features and to support data interpretation. Processing of converted-wave energy (e.g., Barzaghi et al., 2002) may also enhance our ability to extract additional information about subbasalt structures contained in seismic reflection data.

Figure 1 shows the location of the study area between the Faroe and the Shetland Islands, which is of particular interest for the hydrocarbon industry. A key factor in assessing the hydrocarbon potential in this area is the exploration of traps in Mesozoic and lowermost Cenozoic subbasalt sediments, including anticlines and domes in the Faroe-Shetland Basin and tilted fault blocks from Mesozoic rifting. This region has been investigated with the Faroe Large Aperture Research Experiment (FLARE). An overview of the acquisition and processing strategy of the FLARE-project is presented by White et al. (1999). The FLARE-experiment comprises 12 2D wide-angle seismic reflection profiles. It was designed to acquire long-offset reflection and refraction data sets, which enabled a detailed regional study to be made of the geologic structure between the Faroe and Shetland Islands and led to a comprehensive image of the crustal structure (White et al., 2003). For this paper we revisited data recorded along the FLARE-2 seismic reflection profile to test and verify a new approach for subbasalt imaging.

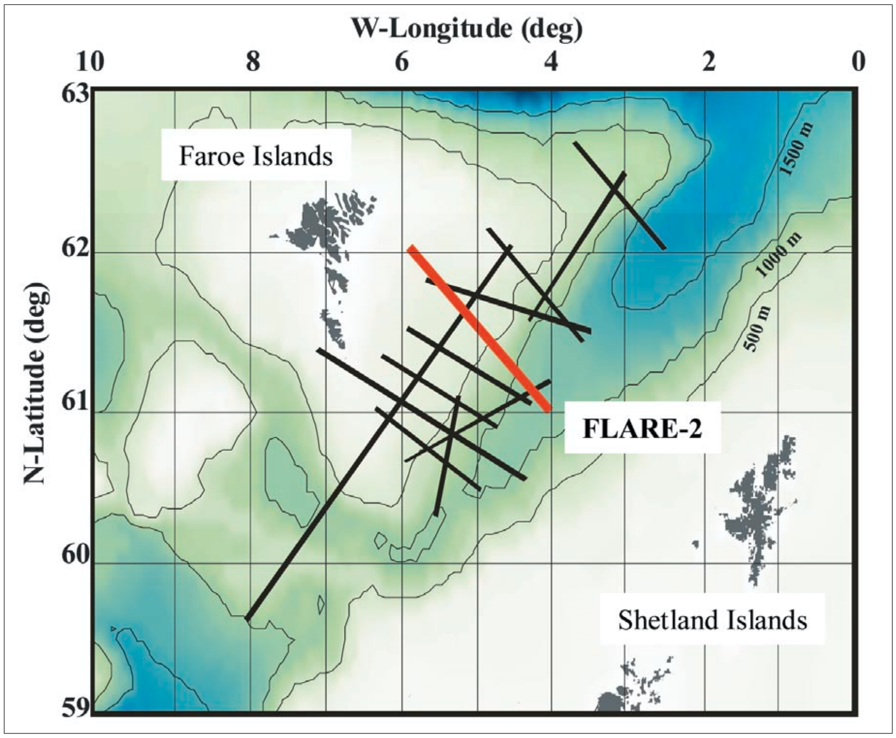

Figure 1. Location of long-offset two-ship profiles comprising the FLARE project southeast of the Faroe Islands. Data acquisition was undertaken by Western Geophysical and the Amerada Hess Limited Partner Group—Amerada Hess, LASMO (ULX), Norsk Hydro, and DOPAS—in the summers of 1996 and 1998. Bathymetric contours in 500-m intervals. Solid black lines indicate the 12 FLARE profiles; bold red line marks location of seismic reflection data recorded along FLARE-2, which are used in this study.

The new technique we introduce is based on the treatment of prestack seismic reflection data in the parabolic τ-p domain. In our processing sequence (Table 1), we "rescale" and filter intrabasalt and subbasalt data in the parabolic τ-p domain to increase significantly the strengths of primary reflections relative to coherent noise (e.g., multiples and converted-wave energy). We demonstrate that a composite image of sediments above the basalt (hereafter referred to as suprabasalt sediments/sequence) obtained from conventional seismic processing and subbasalt features obtained from the proposed τ-p processing yields a comprehensive image of the subsurface. Furthermore, compared to conventional processing this approach strengthens the interpretation of weak intrabasalt and subbasalt features. To illustrate the basic concept, we first apply the τ-p scheme to a CMP gather simulated from a simple 1D velocity model. Finally, the τ-p scheme is used to process the data recorded along the FLARE-2 seismic reflection profile.

Table 1. *Processing scheme in the parabolic τ-p domain. Option A yields appropriate data for velocity analyses. Option B leads to the final stack*

Optional τ-p processing	*Remarks*
NMO-corrections	*using extrapolated top-basalt velocities*
Mute of prestack supra-basalt sequence	
Parabolic τ-p transformation	*limited slowness and frequency ranges*
Square data in τ-p domain	
Filter in τ-p domain	*define reject region and taper in τ-direction*
Inverse parabolic τ-p transformation	*generalized discrete Radon transformation*
Square-root data in t-x domain	*minimize amplitude distortion*
Inverse NMO-corrections	*using extrapolated top-basalt velocities*
→ **OPTION A**	
→ **OPTION B**	
OPTION A - velocity analysis	*output data for final velocity analysis*
OPTION B - final stack	
NMO-corrections, stretch mute, stack	*using updated velocity field*
Recombine with poststack supra-basalt sequence	*overlap depending on intra-basalt data quality*

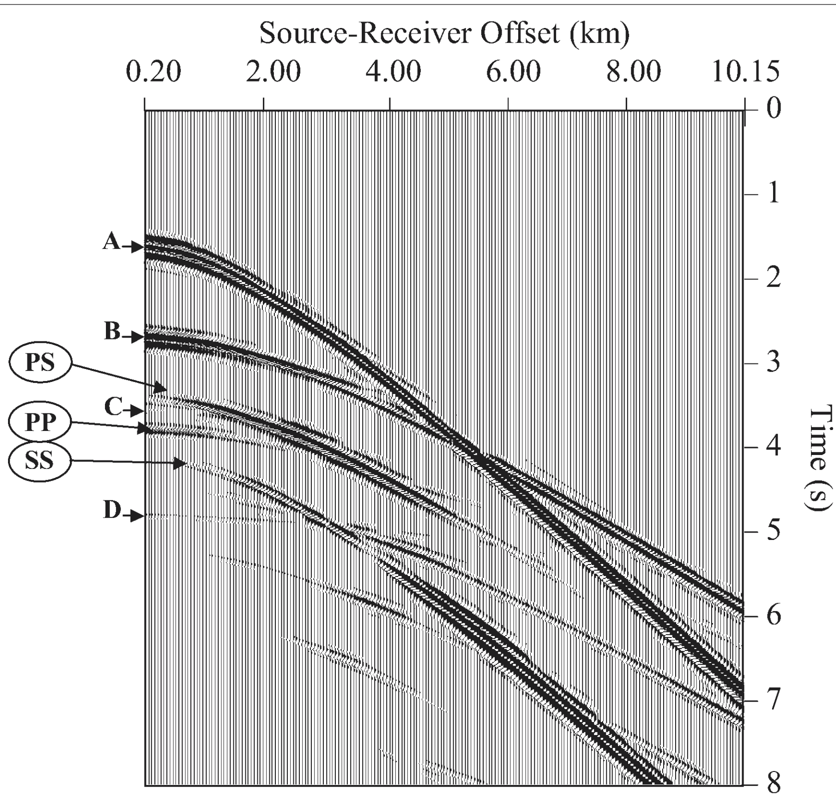

Figure 2. CMP gather simulated using a reflectivity code obtained from simple horizontally stratified 1D velocity model. 200 receivers are spaced at 50-m intervals along the surface. The source pulse is a Ricker wavelet with 20-Hz center frequency (200 m from first receiver). Geometrical spreading corrections, inverse Q-filter, and trace balancing have been applied. Annotations on left side mark primary reflections from interfaces: A = seafloor, B = top-basalt, C = base-basalt, D = basement. Circled labels denote converted-wave arrivals (i.e., PS = downgoing P-wave and upgoing S-wave; SS = down- and upgoing S-wave) from the top-basalt boundary, and PP indicates a first-order P-wave multiple from S1 sediment layer. No water bottom multiples are simulated. Note relatively poor amplitudes of subbasalt reflections C and D.

Synthetic data example. We consider a simple 1D velocity model which approximately represents the subsurface beneath the Faroe-Shetland Basin. The model consists of five plane layers (Table 2): a water layer (W), followed by suprabasalt sediments (S1) on top of a relatively thick basaltic sequence (Ba), which cover subbasalt sediments (S2) and the underlying basement (Bm). The petrophysical parameters characterizing those layers are derived from various studies including borehole measurements and seismic investigations. The relatively low effective quality factor of 30 for the basalt layer accounts for the attenuation of seismic energy within the basalts caused by internal multiple scattering. For simplification and because water-bottom multiples are relatively easy to eliminate from real data, we exclude them from our modeled data.

Figure 2 illustrates a CMP gather for the 1D velocity model calculated using a full-waveform reflectivity code. After applying time- and offset-varying amplitude scaling, the strongest arrivals in the CMP gather are the events from the seafloor and the top-basalt boundary (i.e., primary P-wave arrivals from interfaces A and B). On the other hand, amplitudes of primary subbasalt P-wave reflections from interfaces C (i.e., base-basalt) and D (i.e., basement) are relatively small. This is typical for data recorded in such an environment, where most of the energy is reflected at the top of the basaltic layer and scattered (attenuated) within the basalt. The CMP gather also contains converted wave energy (PS in Figure 2; P-to-S conversion at the top-basalt boundary) and S-wave energy (SS in Figure 2; conversion at the seafloor) travelling through the S1 sediment layer. Further, note that ~200 ms below the base-basalt reflection (C) a strong event (~2 times the amplitude of C) is present, which is the first-order P-wave multiple reflection (PP), bouncing between the seismically hard top and bottom boundary of the sediment layer S1. This event could be easily mistaken for the base-basalt reflection.

To examine the effects of the proposed *τ-p* processing sequence in detail, we enlarge parts of the synthetic CMP gather (Figure 3a). The indices on the left mark the reflections of primary interest (same annotation as in Figure 2). Figure 3b shows the P-wave interval velocity function (solid line) and the rms velocity function (dashed line) for the synthetic 1D velocity model. First-order estimates of suprabasalt velocity variations in observed data are

Table 2. *Synthetic model parameters typical for seismic rock properties along the southeastern part of FLARE-2, where V_P and V_S are P- and S-wave velocities and Q_P and Q_S are Quality factors for P- and S-waves, respectively, ρ is density, and D is thickness of each layer*

		V_P (m/s)	V_S (m/s)	$Q_P = Q_S$ (-)	ρ (kg/m³)	D (m)
Water	W	1500	0	500	1000	1200
Sediment	S1	2200	950	50	2000	1200
Basalt	Ba	4800	2600	30	2500	2100
Sediment	S2	4000	2100	100	2400	2500
Basement	Bm	5500	3200	150	2700	∞

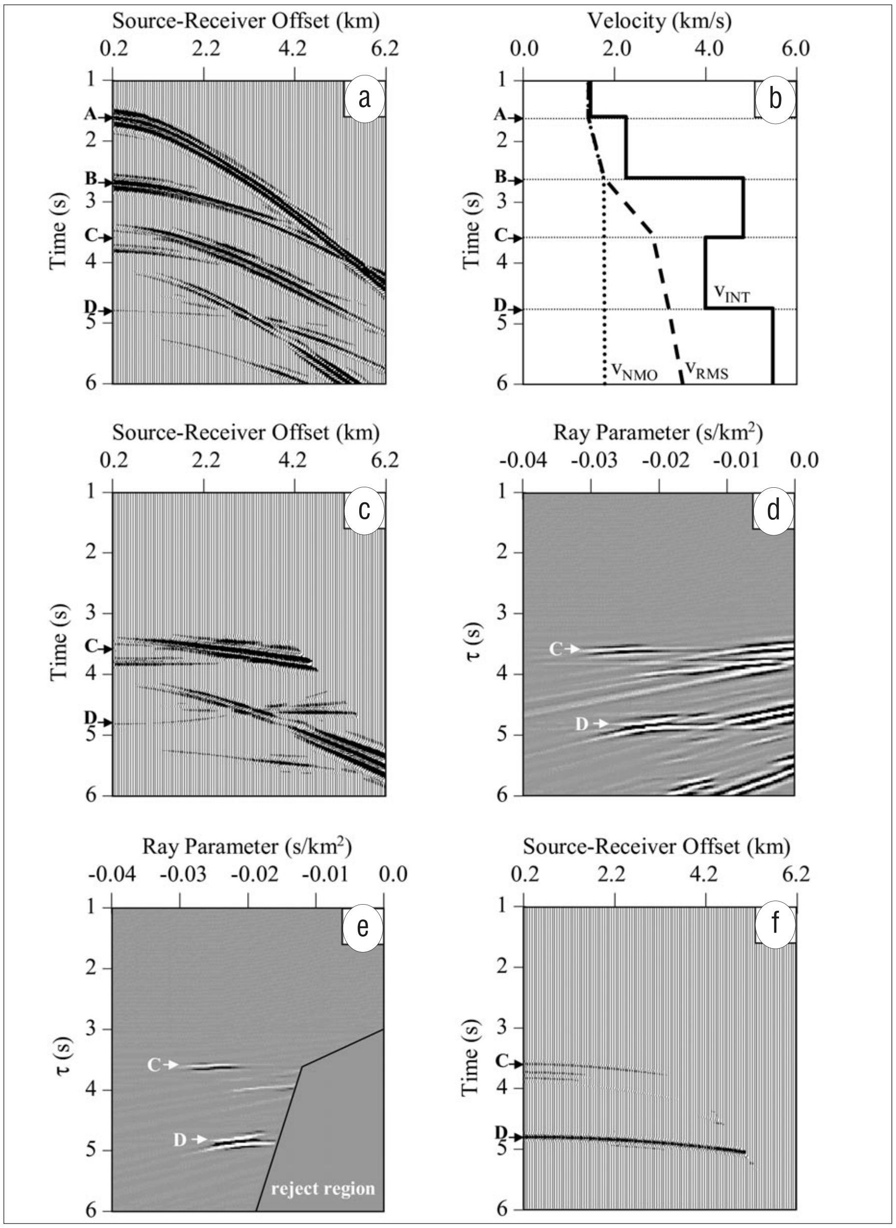

Figure 3. *(a) Enlargement of data in Figure 2. (b) Velocities derived from 1D velocity model, where v_{INT} is interval velocity (bold line), v_{RMS} is rms velocity (dashed line), and v_{NMO} (dotted line) is velocity function used for NMO-corrections. (c) Same as (a), except NMO-corrections and top-mute applied. (d) Result of parabolic τ-p transformation applied to (c), with ray parameter $p = \Delta T/x^2$ (ΔT = moveout, x = source-receiver offset). Reflected signal-to-coherent noise ratio (S/N) is about 10. (e) Same as (d), except amplitude of each sample is squared (sign is preserved), such that S/N is about 100. Same plot scaling applied to (d) and (e); each trace is normalized with respect to the maximum amplitude of the respective section. Black line outlines reject region of filter designed and applied in parabolic τ-p domain to suppress remaining coherent noise. (f) Inverse parabolic τ-p transformation of (e) followed by square rooting every sample value in the t-x domain (again, sign is preserved) and inverse NMO-corrections yields CMP gather with dominant hyperbolic subbasalt reflections.*

provided easily by conventional velocity analyses. The estimation of intra- and subbasalt seismic velocities with standard semblance analyses can be difficult. Therefore, in the *τ-p* processing strategy, the subbasalt velocities are set to time-invariant functions based on velocity estimates obtained from the top-basalt reflections—i.e., v_{NMO} (dotted line in Figure 3b). These time-invariant velocities have no petrophysical meaning for the subbasalt reflections. However, NMO-corrections using these velocity functions convert hyperbolic intrabasalt and subbasalt events into approximately parabolic events.

The application of NMO-corrections using v_{NMO}, followed by muting the suprabasalt data (i.e., top-mute based on two-way-traveltimes to the top-basalt reflection; picked on conventionally processed data) yields data with slightly overcorrected reflections in the *t-x* domain (Figure 3c), which map to smeared points in the parabolic *τ-p* domain (Figure 3d). Theoretically, the parabolic *τ-p* transformation converts parabolic events in the *t-x* domain to points in the parabolic *τ-p* domain. However, *τ-p* transformation applied to real data is always accompanied by smearing effects (i.e., butterfly-shaped features in Figure 3d representing the reflections), which result from the finite length and discretization of recorded data and clustering of summation paths near zero offset. To minimize this effect in the *τ-p* domain and associated amplitude distortions after inverse transformation, we use generalized discrete Radon transforms.

Converted-wave energy and multiples show relatively large positive moveout compared to reflections (Figure 3c) and would therefore map to smeared points in the positive regions of the parabolic *τ-p* domain. For conventional *τ-p* transformations, the relative amplitudes of each ray parameter (i.e., slowness) are independent of the size of the analysis windows, as long as the signal of interest is completely included. Thus, by limiting the range of slownesses from -0.04 s/km² to 0.0 s/km² during parabolic *τ-p* transformation, multiples and other slow-travelling coherent events (e.g., converted wave energy) are largely eliminated.

Nevertheless, remnants of coherent noise are still present in the data and cover primary signal. Note the remaining signal spreading over the entire slowness range in Figure 3d. Summing along parabolic trajectories increases the reflected signal-to-coher-

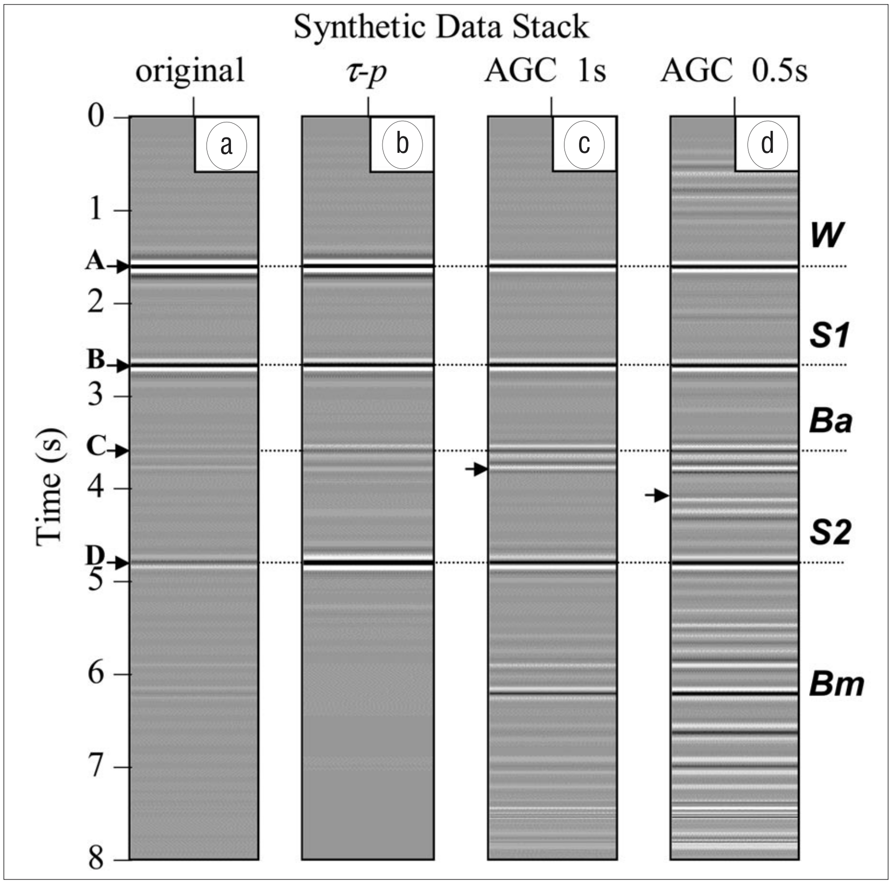

Figure 4. Comparison of stacked data obtained from NMO-corrected (a) original synthetic data and (b) with τ-p processing applied. (c) and (d) Same as (a), after AGC, where operator lengths are (c) 1 s and (d) 0.5 s. Note the relatively high S/N ratio in the τ-p processed section compared to conventional time-variant amplitude scaling.

Table 3. *Principal acquisition parameters of FLARE-2. For details see Fruehn et al. (1998). Only source-receiver offsets up to 12 km have been used in this study*

Number of channels	380
Nominal shot spacing	100 m
Nominal receiver spacing	100 m
Nominal minimum offset	200 m
Nominal maximum offset	38 200 m
Sampling interval	4 ms
Record length	18 s

ent noise ratio (S/N) to ~10 and, therefore, these remnants have much lower amplitudes than the reflections. By simply squaring the value of each sample in the parabolic *τ-p* domain, while maintaining its sign, the S/N is increased further to ~100 (Figure 3e). Note that the same plot scaling has been applied to Figures 3d and 3e.

In addition to the rescaling, it is relatively easy to define a filter in the parabolic *τ-p* domain that further reduces the effects of coherent noise. After setting amplitudes inside the reject-region of the *τ-p* filter (Figure 3e) to zero and applying a 100 ms taper in the *τ-p* direction, inverse parabolic *τ-p* transformation is performed. Subsequent calculation of the square root of the inverse transformed values followed by removal of NMO-corrections yields the CMP gather of Figure 3f. Most coherent nonprimary events are eliminated over the entire source-receiver offset range, without affecting noticeably the primary reflections. Reflections from interfaces C and D are now the strongest events on the CMP gather. To allow the amplitudes and general appearance of reflections before and after *τ-p* filtering to be compared directly, all CMP gathers in Figure 3 are displayed with the same time- and offset-varying amplitude scaling function. The final CMP data (Figure 3f) can either be subjected to another velocity analysis (option A in Table 1) or be stacked and merged with conventionally processed suprabasalt poststack data (option B in Table 1).

In Figure 4 we examine the effect of the proposed *τ-p* scheme on the amplitudes of stacked synthetic seismic data (option B in Table 1) and we compare the outcome with the result obtained from conventional scaling—i.e., automatic-gain-control (AGC). Merging of the suprabasalt data and the *τ-p* processed data is performed on poststack data, since the overlap (taper) between the two is easier to define on poststack sections than on prestack CMP gathers. The base-basalt reflection (C) is almost invisible on the stacked unfiltered data (Figure 4a) even in this synthetic case with no noise present, whereas the rescaling and filtering process in the parabolic *τ-p* domain yields enhanced stacked data without amplifying nonprimary events (Figure 4b). After applying a simple AGC with 1-s operator length instead of *τ-p* processing, the nonprimary events are also enhanced (Figure 4c). Note that ~200 ms below C the first-order P-wave multiple reflection from the S1 sediment layer (Figure 2) is significantly enhanced (arrow in Figure 4c). This nonprimary reflection shows the same amplitude as the primary reflection C, erroneously gained by the AGC. Furthermore, the shorter the operator length of the AGC, the more effect it has on the stacked data (compare Figures 4c with 4d). With an AGC operator length of 0.5 s, even converted-wave energy (arrow in Figure 4d) and other coherent noise (i.e., including numerical artifacts from the simulation in this example) reach the same amplitude level as primary reflections. This is unacceptable and can be avoided by applying our proposed rescaling and filtering scheme in the parabolic *τ-p* domain.

Finally, three observations need to be considered when using the proposed scheme:

1) It is important to mention that some amplitude information is changed during the processing in the parabolic *τ-p* domain. Even though a generalized discrete Radon transform has been used, which minimizes differences between input and output data sets in a least-squares sense, squaring the data in the parabolic *τ-p* domain and subsequent square-rooting in the *t-x* domain results in alterations of absolute amplitudes. However, relative amplitude variations along and between individual subbasalt reflections are preserved, as we would expect.
2) Squaring the data in the parabolic *τ-p* domain leads to a substantial increase in S/N ratio; so, why not use higher powers? Our experience suggests that employing higher powers on this data set results in greater amplitude distortions. Furthermore, higher powers would increase the differences between strong and weak

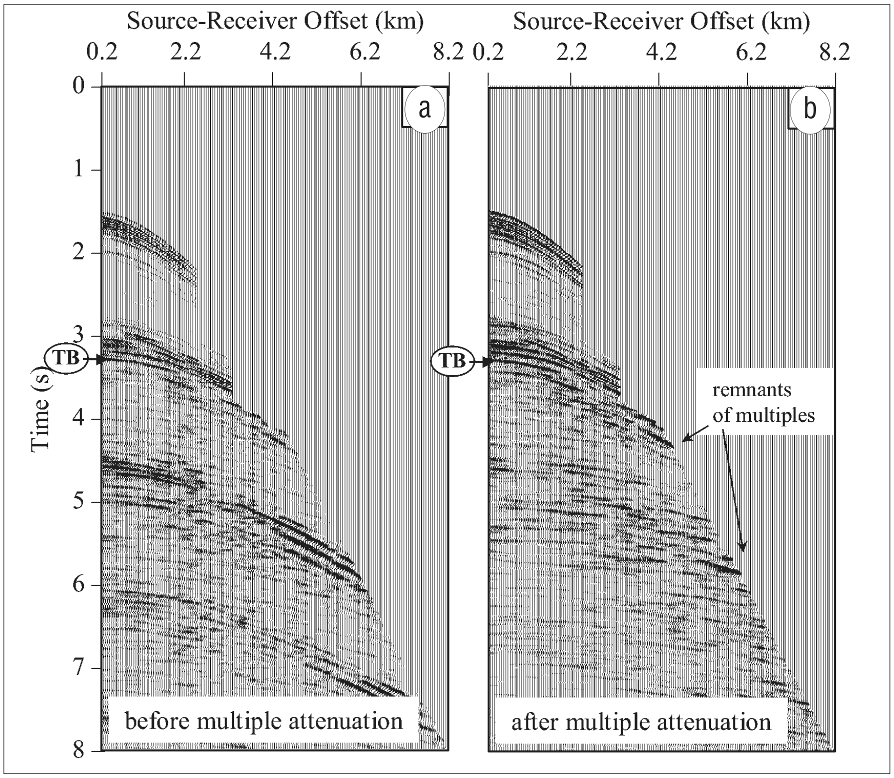

Figure 5. *(a) Typical CMP gather recorded along FLARE-2 profile after scaling and signal enhancement applied. Trace spacing is uniformly 50 m. Relevant top-basalt reflection (TB) becomes evident at ~3.3 s. Subbasalt reflections are poorly resolved and mostly obscured by multiple energy. (b) Same as (a) after three-step sequence for multiple attenuation applied, which markedly improves the appearance of subbasalt events.*

Table 4. *Processing sequence applied to seismic reflection data recorded along FLARE-2, which includes optional τ-p processing outlined in Table 1*

Scaling and signal enhancement:
Geometric spreading correction
Inverse Q-filter
Band-pass filter
Predictive deconvolution
Flex-binning
f-x-interpolation
Multiple attenuation:
Wave equation multiple modeling
Predictive deconvolution in linear *τ-p* domain
Mute in parabolic *τ-p* domain
Initial velocity analysis
Kirchhoff prestack time migration
Optional *τ-p* processing (Table 1 — OPTION A)
Final velocity analysis
Optional *τ-p* processing (Table 1 — OPTION B)

reflected signals and, hence, lead to significant suppression of weak reflections in the final result.

3) The overlap between conventionally processed suprabasalt data and the *τ-p* processed subbasalt section depends strongly on the S/N ratio directly below the top-basalt reflection. If the penetration of seismic energy in the basaltic layers is sufficiently deep, the quality of conventionally processed data often shows reasonable resolution in the intrabasalt sequence. In this case, the start of the *τ-p* processed section which is merged with the conventionally processed data can be at later two-way traveltimes.

Field data example. We have tested the new *τ-p* processing strategy on subbasalt seismic reflection data acquired along the FLARE-2 profile southeast of the Faroe Islands. To obtain a comprehensive image of the crustal structure in the Faroe-Shetland area from joint reflection (i.e., near-offset and wide-angle data) and diving-wave data analyses, ultralong offsets (~38 km) have to be recorded. This was achieved by using a two-vessel configuration with relatively coarse shot and receiver sampling of 100 m (Table 3). Since our proposed processing scheme is an advanced strategy for conventionally acquired data, for the purpose of this study we limited the FLARE-2 data set to a single-streamer data set with a maximum source-receiver offset of 12 km.

The acquisition configuration results in a CMP gather trace spacing of 200 m, where adjacent CMP gathers have complementary source-receiver offset distribution. Such sparse sampling in the CMP domain requires trace interpolation before multiple attenuation techniques and the proposed *τ-p* scheme can be applied. This is accomplished with flex-binning followed by *f-x* interpolation, both applied to NMO-corrected CMP gathers. Flex-binning combines three adjacent CMP gathers with complementary source-receiver offset traces and, therefore, yields CMP gathers with 100-m CMP gather trace spacing. Subsequent *f-x* interpolation was applied to further reduce the spatial sampling interval within a CMP gather to 50 m, which is sufficiently dense for the intended data processing.

Table 4 summarizes the entire processing sequence applied to the FLARE-2 data set—conventional preprocessing (including aforementioned trace interpolation) and optional processing in the *τ-p* domain. Careful suppression of multiple reflections is generally critical in marine seismic data processing, and numerous articles have been published about this topic. For the successful imaging of subbasalt features, it is even more important to set up an appropriate strategy for minimizing multiple events. Since reflections from the intrabasalt and subbasalt regions are expected to be extremely weak, incomplete elimination of multiples may easily lead to misprocessing and their misinterpretation as primary reflections.

A successful example of suppressing multiple energy in the presence of a hard reflector is shown by Matson et al. (1999). This strategy combines three different techniques, each of which addresses multiple events of diverse origin. After extensive testing we decided to apply such a three-step sequence, which consists of (1) wave-equation modeling, (2) predictive deconvolution in the linear *τ-p* domain, and (3) muting in the parabolic *τ-p* domain. Wave-equation modeling effectively removes the water-bottom multiple through wavefield prediction and subtraction. Predictive deconvolution in the linear *τ-p* domain, using an operator length and prediction distance dependent on the two-way traveltime between the seafloor and top-basalt (i.e., TWT), successfully suppresses multiples generated between those two boundaries. The predictive

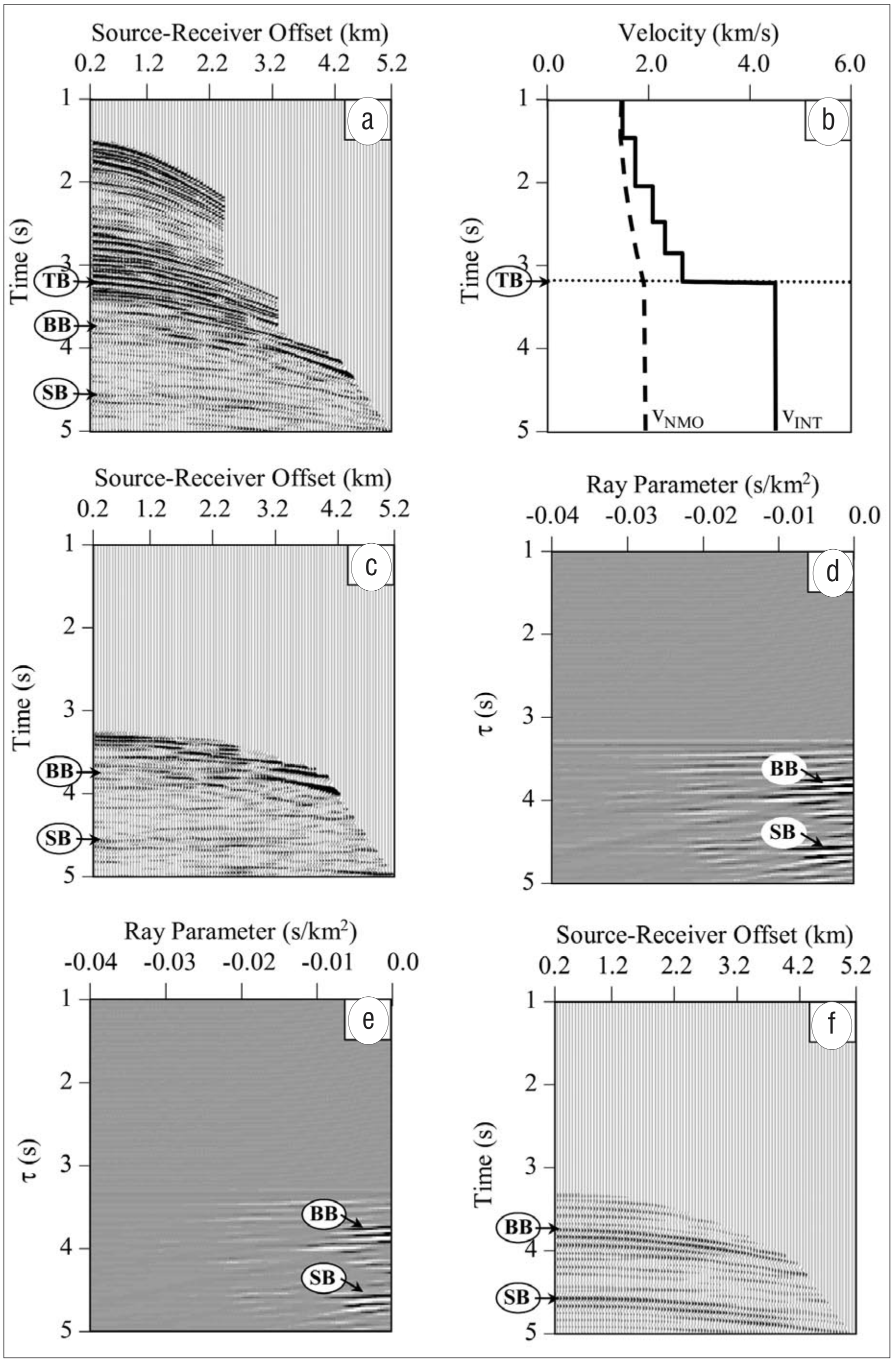

Figure 6. *(a) Enlargement of data in Figure 5b. Annotations on left mark top-basalt reflection (TB), interpreted base-basalt boundary (BB), and a prominent subbasalt event (SB). (b) Velocities obtained from standard velocity analysis using suprabasalt seismic data, where v_{INT} is interval velocity and v_{NMO} is rms velocity used for NMO-corrections. Dotted line marks top-basalt boundary. (c) As for (a), except NMO-corrections and top-mute based on top-basalt reflection applied. (d) Result of parabolic τ-p transformation applied to (c). (e) Same as (d), except amplitude of each sample is squared (sign is preserved). Same plot scaling applied to (d) and (e); each trace is normalized with respect to the maximum amplitude of the respective section. Note reduced noise (i.e., nonprimary signal) level in (e) relative to (d). (f) Result of inverse parabolic τ-p transformation followed by square rooting every sample value (again, sign is preserved) and inverse NMO-corrections applied to (e); intrabasalt reflections, base-basalt horizon and subbasalt events are markedly enhanced. Identical trace balancing applied to Figures 6a, 6c, and 6f.*

deconvolution operator length is 2.5 × TWT and the prediction distance is 0.5 × TWT. Finally, careful muting in the parabolic *τ-p* domain reduces remaining multiple energy. Figure 5 shows a typical trace-normalized CMP gather recorded along the FLARE-2 profile before and after multiple attenuation. Strong events from suprabasalt sediments (~1.5-3.3 s) are observable in both panels. Amplitudes of reflections from the basaltic sequence and from interfaces below the basalt become clearer after multiple attenuation. However, these reflections are relatively weak and are partly obscured by remaining multiple energy. Therefore, it is essential to enhance primary reflections relative to multiple reflections and nonreflected energy in the subbasalt part of the data.

Figure 6a shows an enlarged area of the data in Figure 5b after Kirchhoff prestack time migration. TB indicates the top-basalt boundary, which separates suprabasalt sediments from intra- and subbasalt events. This horizon and the suprabasalt reflections are the most prominent features in conventionally processed data and can easily be followed throughout the entire migrated section. The weak appearance of the interpreted base-basalt reflection (BB) and various subbasalt reflectors (SB) prevent successful imaging of these events. The same observation applies for velocity analysis; standard semblance analyses yield excellent estimates for suprabasalt sediments and the top-basalt reflection, whereas poor data quality in intra- and subbasalt regions prevents accurate estimation of seismic velocities. Figure 6b illustrates interval velocity and stacking velocity derived from the CMP gather in Figure 6a. Velocity estimates below the top-basalt reflection are assumed constant. Applying NMO-correction using this velocity function followed by muting the suprabasalt sequence yield intra- and subbasalt data with slightly overcorrected parabolic events in the *t-x* domain (Figure 6c). These events image to smeared "points" after parabolic *τ-p* transformation (Figure 6d). As for the synthetic data, the range of slowness for the *τ-p* transformation is limited to suppress remnants of multiple energy effectively.

To accommodate the low-frequency content of the subbasalt signal, the range of frequencies is also limited. The complex internal impedance structure of the basaltic sequence causes strong attenuation of high-frequency components, and therefore the received subbasalt signal in recorded data is generally dominated by low frequencies. Our experience shows that the frequency content of the useful seismic signal barely exceeds 20 Hz. Therefore, we also restrict the range of frequencies to 0-20 Hz for the parabolic *τ-p* transformation, which yields a clearer image of reflected events in the parabolic slant stacks, without affecting the waveform of the subbasalt signal. Subsequent squaring each sample value in the *τ-p* domain markedly enhances the reflections relative to other events (Figure 6e). Note that the reject region

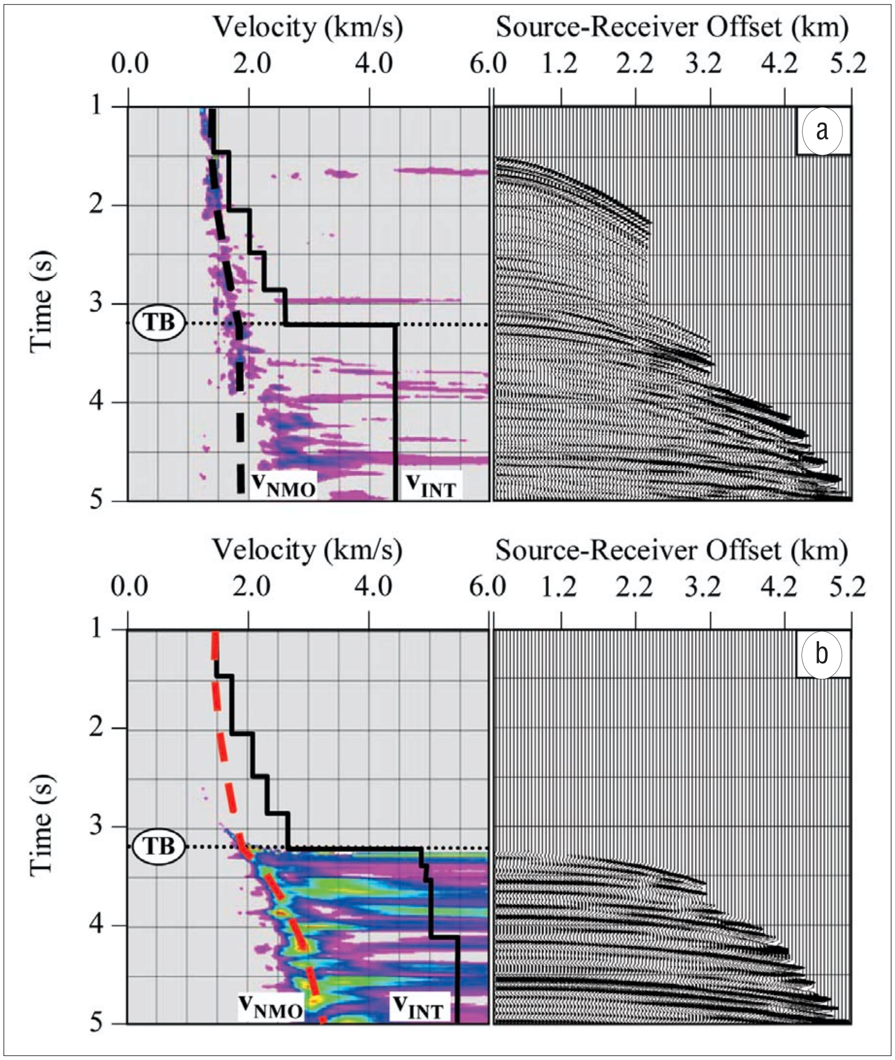

Figure 7. Semblance plots (left) derived from CMP supergathers, composed of five adjacent CMP gathers (right). For display purposes, traces have been scaled with 1000 ms AGC. (a) CMP supergather contributed to the initial velocity analysis. (b) Same as (a), except τ-p processing has been applied. This CMP supergather contributed to final velocity analysis. Dotted line marks top-basalt boundary, black bold line indicates estimates for interval velocity v_{INT}, black dashed line in (a) illustrates v_{NMO} used for NMO-corrections in optional τ-p processing. Red dashed line in (b) denotes final stacking velocity function.

of the *τ-p* filter (Figure 3a) starts at ~5.5 s and, therefore, is not shown in Figure 6e. Inverse parabolic *τ-p* transformation, followed by square-rooting every sample value and inverse NMO-corrections, yields a CMP gather with prominent primary base- and subbasalt reflections (Figure 6f). The rescaling and filtering process has markedly increased the subbasalt signal compared to conventionally processed data, while maintaining relative amplitudes along and between individual reflections (compare Figure 6a with 6f).

When comparing the intrabasalt sequences in Figures 6a and 6f (~3.3-3.7 s), the conventionally processed data (Figure 6a) show better resolution since the penetration of seismic energy into the basaltic layer is sufficiently deep. The limitation of the frequency range for the parabolic *τ-p* transformation reduces the resolution in the intrabasalt time range of the *τ-p* processed CMP data (Figure 6f). As mentioned above, the conventionally processed suprabasalt section will therefore be extended to later two-way traveltimes.

As shown in Table 4, we have applied the *τ-p* scheme twice, once to obtain CMP data for more accurate subbasalt velocity analyses (option A in Tables 1 and 4), and once to increase the S/N ratio in the final migrated section (option B in Tables 1 and 4). Figure 7 illustrates the differences between a CMP supergather without further processing (Figure 7a) and after the application of *τ-p* processing (Figure 7b). After *τ-p* processing, stacking velocities can be estimated with more confidence (compare left panels in Figure 7). The final velocity picks (red line in Figure 7b) are based not only on the semblance plot, but also on the NMO-corrected CMP supergather and ministacks (neither is shown here). Finally, Figure 8 illustrates how the combination of suprabasalt data and *τ-p* processed intra- and subbasalt data is realized (option B in Tables 1 and 4). Figure 8a shows the result of conventional processing applied to suprabasalt data along a 500-m segment of the FLARE-2 profile. The top-basalt reflection (TB) is clearly observed as a continuous event on the conventionally processed section. The two-way traveltimes to this reflector plus a taper set the bottom-mute times for the conventionally processed suprabasalt sequence. The taper length depends on the quality of the intrabasalt image; deeper penetration of relatively high-frequency seismic energy yields better quality of the intrabasalt seismic image and, therefore, a greater taper length allows more conventionally processed data to be included in the final image. The taper length along the entire profile varies between 1000 ms (northwestern part of FLARE-2) and 600 ms (southeastern part of FLARE-2). The taper length for the subbasalt part of the data is 100 ms along the entire profile. Figure 8b shows the result of the *τ-p* processed subbasalt section and Figure 8c illustrates the result of combining the data shown in Figures 8a and 8b. For comparison purposes the relevant section obtained from standard processing is presented in Figure 8d. The interpreted base of the basalt (BB) and the underlying interpreted basement boundary (Bm) can hardly be recognized on the standard section (Figure 8d), but Figure 8c shows improved continuity, increased S/N ratio and the clear change of the reflection characteristics. This enables a confident interpretation of the base-basalt reflection and mapping of the basement boundary.

Comparison with conventionally processed seismic reflection data. We have shown that processing applied in the parabolic *τ-p* domain has the potential to improve significantly the signal-to-noise ratio in subbasalt data (compare Figure 6a with Figure 6f and Figure 8c with Figure 8d). To examine the effects of these improvements on final seismic images, we have processed the entire FLARE-2 data set twice, once using conventional time processing and a second time including the proposed *τ-p* strategy for the subbasalt part of the data. Figure 9a shows the migrated section obtained from standard time processing. Figure 9b shows the result of applying the strategy with the parabolic *τ-p* processing scheme. Except for the optional *τ-p* processing we used the same processing

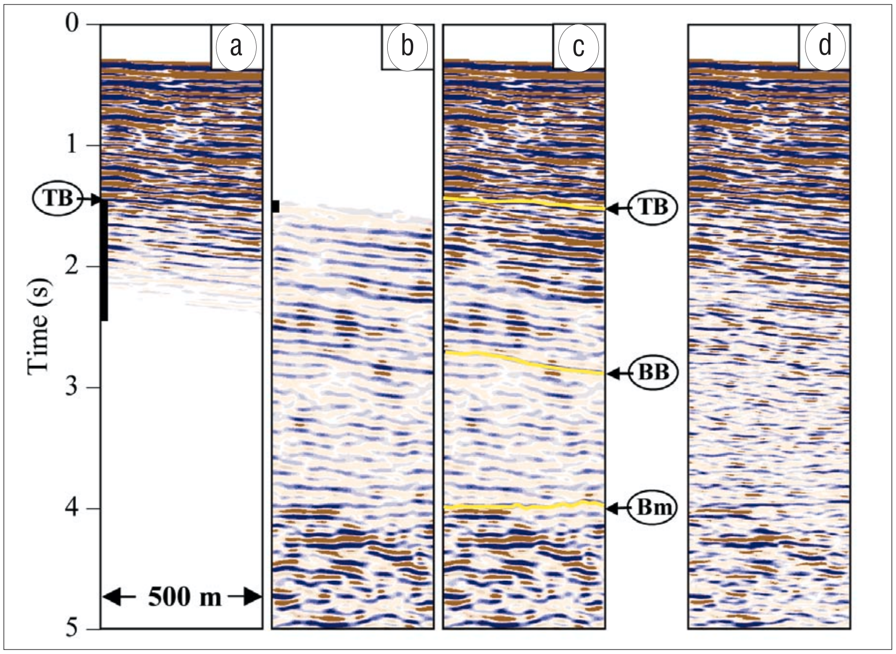

Figure 8. (a) Conventionally processed suprabasalt sequence. (b) Subbasalt data with optional τ-p processing applied. (c) Result of merging (a) and (b) with tapers of 1000 ms applied to the suprabasalt section and 100 ms applied to the subbasalt section; taper lengths indicated by black bars on the left of individual sections. (d) Result of conventional processing applied to the entire section. Note that the base-basalt reflection and the basement boundary are not as clearly seen as after τ-p processing. Same annotation as in Figure 6; Bm indicates interpreted basement reflection.

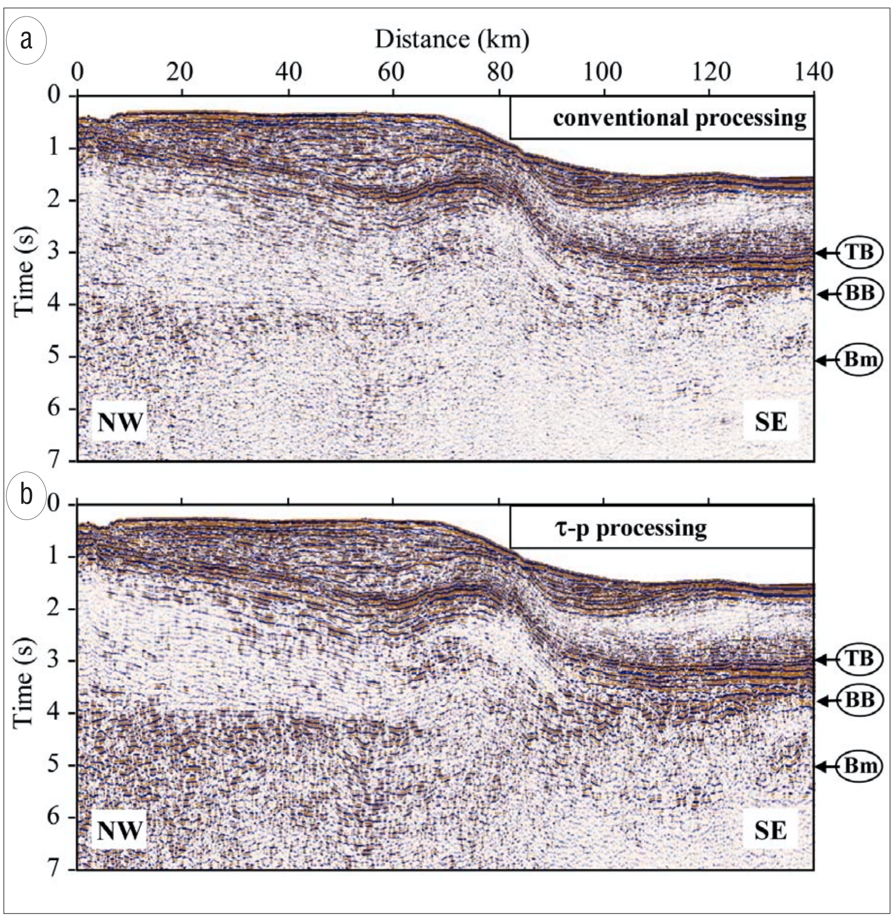

Figure 9. Kirchhoff prestack time-migrated sections obtained by (a) applying conventional processing, and (b) merged with intra- and subbasalt data obtained from optional τ-p processing. Identical trace balancing applied to both sections. Except for the optional τ-p processing, the same processing sequence with identical parameters was employed for both sections. Note enhancement of subbasalt signal, especially reflections indicating the basement (~4 s).

sequence with identical processing parameters for the two sections. Differences between the sections in Figures 9a and 9b are solely a function of these optional processing steps in the parabolic *τ-p* domain. The advantages of the new strategy for mapping subbasalt structures are particularly evident. Subbasalt reflections on the *τ-p* processed section are uniformly more continuous than those on the conventionally processed data and portions of the intra- and subbasalt features become more visible after *τ-p* processing has been applied. Furthermore, the interpreted basement at ~4 s is seen clearly on the *τ-p* processed section, whereas it is hardly recognizable on conventionally processed data.

Comparison with prestack depth-migrated wide-angle seismic reflection data. Recent studies in the Faroe-Shetland area (Fruehn et al., 2001, and White et al., 2003), focusing on separate processing of near-offset and wide-angle seismic reflection data yield excellent estimates of the base-basalt and subbasalt reflections along the FLARE-2 data set. Applying Kirchhoff prestack depth migration to carefully selected large-aperture seismic reflection data comprising the full source-receiver offset range up to 38 200 m of the FLARE-2 profile, clearly reveals the base of the basalt (BB in Figure 10a). Details of the processing strategy are given in White et al. (2003). The superimposed interpretation in Figure 10a (yellow lines) indicates top-basalt (TB) and base-basalt (BB) boundaries from White et al. (2003).

Comparison of Figure 10a with the result obtained from our proposed strategy followed by simple time-to-depth conversion (Figure 10b) illustrates the strength of *τ-p* processing; wide-angle processing focuses on accurate mapping of specific boundaries (e.g., base-basalt), while the proposed *τ-p* processing improves the resolution of the full depth range below the top-basalt horizon. Note that the two faults which appear to cut through the entire basalt sequence (arrows in Figure 10b) are only resolved after *τ-p* processing has been applied (Figure 10b).

Interpretation of major geologic units. Figure 11 illustrates the interpretation of the major geologic units observed along the *τ-p* processed FLARE-2 profile. The suprabasalt sequence (S1) can be clearly distinguished from the underlying basaltic sequence (Ba). They are separated by a strong continuous reflection from the top of the basalt. The Tertiary flood basalts themselves can be divided into an upper section characterized by

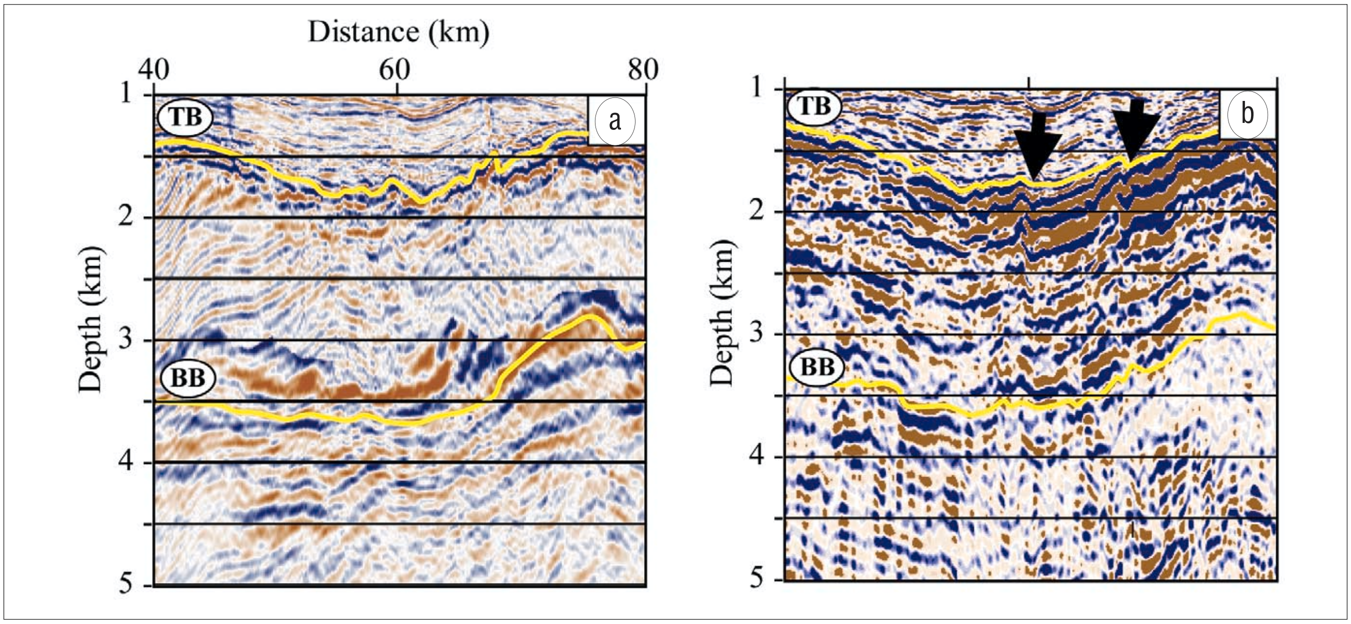

Figure 10. (a) Prestack depth migration obtained from wide-angle data (figure adapted from White et al., 2003). (b) As Figure 9b, except time-to-depth conversion applied. Yellow lines indicate top-basalt reflections (TB) and base-basalt reflections (BB), respectively, picked on individual seismic sections. Black arrows in Figure 10b denote faults within the basaltic sequence. Top annotation illustrates location within the FLARE-2 profile (compare with Figure 9).

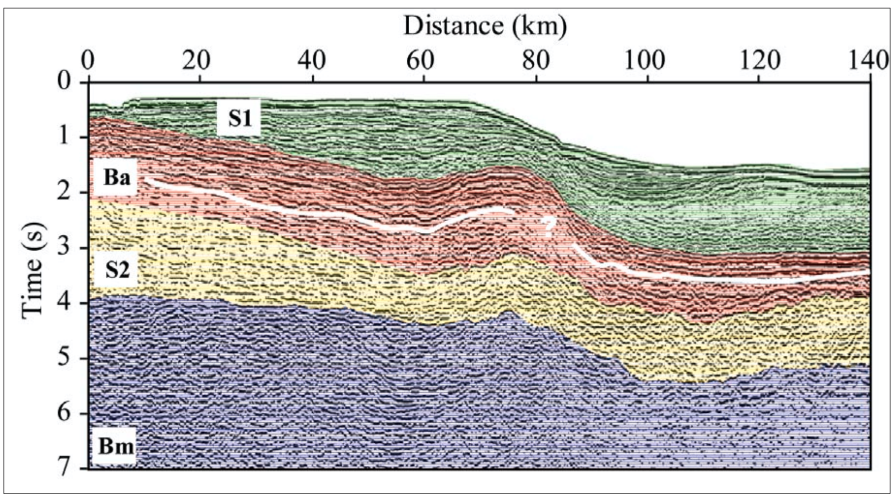

Figure 11. Same as Figure 9b, with interpretation superimposed. S1 = suprabasalt sediments (green); Ba = basaltic sequence (red); S2 = subbasalt sediments (yellow); Bm = basement (blue). For details of interpretation see text.

continuous subbasalt reflections and a lower section characterized by a hummocky reflection pattern, each of which comprise about half of the total thickness of the basalt sequence.

The white line in Figure 11 indicates the boundary between these two types of basalt. The subbasalt sediments (S2) are clearly separated from the basalt above them and the interpreted basement (Bm) below. The hummocky reflection pattern of the lower section of basalts changes to low reflectivity within the S2 sediments, which are then bounded beneath by a strong reflection from the basement, particularly on the northwestern part of the FLARE-2 profile. The basement itself is characterized by an increase in reflectivity compared to the overlying sediments and by semicontinuous reflections. Detailed information about the general development of the basin is supplied by White et al. (2003); implications for petroleum exploration are published in Doré et al. (2002).

Conclusions. Our ability to image seismically the subbasalt subsurface at many locations worldwide is limited by the fact that basaltic layers are generally characterized by poor seismic penetration for various reasons (including high reflectivity contrast, scattering and attenuation). To address this issue, we propose an efficient processing strategy that enhances reflected seismic energy received from below the top-basalt boundary. We show that rescaling and filtering the data in the parabolic τ-p domain greatly improves the appearance of intrabasalt and subbasalt reflections. Essential elements of this strategy are:

- NMO-corrections with rms velocities obtained from conventional semblance analyses of the top-basalt reflections yield parabolic intrabasalt and subbasalt reflection data.
- Parabolic τ-p transformation of NMO-corrected data with limited ranges of ray parameter and frequency results in further reduction of multiples and converted-wave energy and yields a clearer image in the τ-p domain.
- Rescaling (i.e., squaring) and filtering (i.e., reject filter) the τ-p transformed data increases significantly the reflected signal-to-coherent noise ratio (S/N).
- Inverse parabolic τ-p transformation (generalized radon transform reduces the amount of smoothing and amplitude distortion) followed by square-rooting every sample value and inverse NMO-corrections yields final data for further processing.

We have tested this processing strategy on both synthetic and real data. Transformation of the CMP gathers (Figures 3 and 6) into the parabolic τ-p domain using appropriately broad ranges of slowness and frequency noticeably enhances the S/N ratios. Further increases of this ratio were obtained by squaring sample values and eliminating remnants of coherent noise in the parabolic τ-p domain. Transforming the data back to the t-x domain yields superior data quality compared to conventionally processed CMP gathers. One notable disadvantage of rescaling in the parabolic τ-p domain is a loss of amplitude information. Nevertheless, reflections on the τ-p processed section (Figure 9b) were found to be enhanced and more continuous than those on the conventionally processed section (Figure 9a), and relative amplitude variations along individual reflections are preserved.

Comparison with the result obtained from prestack depth migration of wide-angle data has shown that our proposed processing strategy is accurate and allows better imaging of intra- and subbasalt features. Furthermore, the results presented in this study were obtained from data recorded to source-receiver offsets of only 12 km, which can be achieved using a single streamer configuration, with considerably less effort in the field compared to Fruehn et al. (2001) and White et al. (2003) who used a two-vessel configuration with up to 38 km source-receiver offsets.

We conclude that the suggested τ-p processing strategy is useful for improving the quality of subbasalt images. The results presented in this study underline the importance of advanced seismic reflection data processing. Although the major lithological units can be identified with conventionally processed seismic data, much more detailed images of the subsurface structures and greater confidence in the interpretation are obtained from the τ-p processed data set.

Suggested reading. "Faeroe sub-basalt seismic imaging: a new iterative time processing approach" by Barzaghi et al. (*First Break*, 2002). "Exhumation of the North Atlantic Margin: Timing, Mechanisms and Implications for Petroleum Exploration" by Doré et al. (*Geological Society Special Publications*, 2002). "FLARE—A two-ship experiment designed for subbasalt imaging" by Fruehn et al. (*SEG 1998 Expanded Abstracts*). "Integrated wide-angle and near-vertical subbasalt study using large-aperture seismic data from the Faeroe-Shetland region" by Fruehn et al. (GEOPHYSICS, 2001). "A quantitative study on the use of converted waves for subbasalt imaging" by Hanssen et al. (*Geophysical Prospecting*, 2003). "A comparison of three multiple-attenuation methods applied to a hard water-bottom data set" by Matson et al. (*TLE*, 1999). "Faeroes Large Aperture Research Experiment (FLARE): imaging through basalt" by White et al. (Proceedings of Petroleum Geology Northwest Europe, 1999). "Imaging and regional distribution of basalt flows in the Faeroe-Shetland Basin" by White et al. (*Geophysical Prospecting*, 2003). "Use of low frequencies for subbasalt imaging" by Ziolkowski et al. (*Geophysical Prospecting*, 2003). TLE

Acknowledgments: The FLARE data used in this article were collected by Amerada Hess Limited and its partners LASMO (ULX) Limited, Norsk Hydro a.s., DOPAS, and Atlantic Petroleum. WesternGeco provided the Omega software with which FLARE data were processed. We acknowledge the help of colleagues in the iSIMM (integrated Seismic Investigation and Modeling of Margins) study group which, with the authors, comprises N. J. Kusznir, A. M. Roberts, N. Hurst, Z. C. Lunnon, C. J. Parkin, A. W. Roberts, L. K. Smith, and V. Tymms. iSIMM is supported by the U.K.'s Natural Environment Research Council and Department of Trade and Industry, Agip UK, BP, Amerada Hess, Anadarko, ConocoPhillips, Shell, Statoil, and WesternGeco. Department of Earth Sciences Cambridge contribution number ES.7510.

Corresponding author: roman@esc.cam.ac.uk